Studying Nuclear Effects with Neutrinos

Steve Boyd,[*] Sergey Kulagin,[†] Jorge G. Morfín,[‡] and Ronald Ransome[§]

MINERνA Note 700
October, 2004

1 Introduction

Most neutrino scattering experiments, including neutrino oscillation experiments, require massive nuclear target/detectors to obtain useful reaction rates. Analysis of neutrino reactions with nuclear media requires understanding the nuclear environment's effect on the process [1]. There are two general categories of such nuclear effects:

- The neutrino interaction probability on nuclei is modified relative to free nucleons. Nuclear effects of this type have been extensively studied using muon and electron beams, but have not been explored with neutrinos. Depending on the kinematic region, these nuclear effects can be quite different for neutrinos. This is particularly true for the shadowing phenomenon [2]. In the shadowing region, for a given Q^2 the cross-section suppression due to shadowing occurs for much lower energy transfer (ν) in neutrino interactions than for charged leptons. This is very relevant for the neutrino energies of oscillation experiments.

- Hadrons produced in a nuclear target may undergo final-state interactions (FSI), including re-scattering and absorption. These effects may significantly alter the observed final-state configuration and measured energy [3, 4], and are sizable at neutrino energies typical of current and planned neutrino oscillation experiments [5].

The hadron shower observed in neutrino experiments is actually the *convolution* of these two effects. FSI effects are dependent on the specific final states that, even for free protons, differ for neutrino and charged-lepton reactions. The

[*]University of Pittsburgh and Imperial College London
[†]Institute for Nuclear Research, Moscow
[‡]Fermilab
[§]Rutgers University

suppression or enhancement of the production of particular final states by nuclear effects also differ for neutrino and charged lepton reactions. For these reasons, measurements of nuclear effects with charged leptons cannot be simply applied to neutrino-nucleus interactions.

To study these questions in MINERνA, carbon, iron and lead targets will be installed upstream of the pure scintillator active detector. To measure the overall effect of the nucleus, the observed interaction rate, hadron energy and multiplicity will be measured for all three targets.

2 Modified Interaction Probabilities due to Nuclear Effects

As mentioned, pronounced nuclear effects have been observed in *charged-lepton* scattering off a number of nuclear targets. The experimental situation is discussed in review papers [6, 7].

The mechanisms of nuclear scattering have also been studied theoretically. These mechanisms appear to be different for small and large Bjorken x as viewed from the laboratory system. Bjorken x is defined as $x = Q^2/2M\nu$, where ν and $\boldsymbol{q}$ are energy and momentum transfer to the target and $Q^2 = \boldsymbol{q}^2 - \nu^2$. The physical quantity which is responsible for the separation between large and small x regions is a characteristic scattering time, which is also known as Ioffe time (or length) $\tau_I = \nu/Q^2$ [8]. If τ_I is smaller than the average distance between bound nucleons in a nucleus then the process can be viewed as incoherent scattering off bound nucleons. This happens at larger $x(> 0.2)$.

At small Bjorken x the space-time picture is different. The underlying physical mechanism in the laboratory reference frame can be sketched as a two-stage process. At the first stage the virtual photon γ^* (or W^* or Z^* in case of neutrino interactions) fluctuates into a quark-antiquark (or hadronic) state. This hadronic state then interacts with the target. The uncertainty principle allows an estimate of the average lifetime of such hadronic fluctuation as

$$\tau = 2\nu/(m^2 + Q^2), \tag{1}$$

where m is the invariant mass of the hadrons into which the virtual boson converts. The same scale τ also determines characteristic longitudinal distances involved in the process. At small x, τ exceeds the average distance between bound nucleons. For this reason coherent multiple interactions of this hadronic fluctuation in a nucleus are important in this kinematical region. It is well known that the nuclear shadowing effect for structure functions is a result of coherent nuclear interactions of hadronic fluctuations of virtual intermediate bosons (for a recent review of nuclear shadowing see, e.g., [7]).

2.1 Nuclear effects in the incoherent regime at large x

If x is large enough to neglect coherent nuclear shadowing effect, the lepton scattering off a nucleus can be well approximated as incoherent scattering off bound protons and neutrons. The most pronounced nuclear effects in this region are due to Fermi-motion, nuclear binding [9, 10, 11, 12, 13, 14, 15], and off-shell modification of nucleon structure functions [14, 15, 16, 17, 20].

A widely used approximation in the description of nuclear structure functions is to neglect the final state interactions of produced hadronic states with the recoiling nucleus. In this approximation the nuclear structure functions can be written as the bound nucleon structure function averaged (convoluted) with the nuclear spectral function (for derivation and more details see [11, 14, 20]). Since bound nucleons are off-mass-shell particles their quark distributions generally depend on nucleon virtuality k^2 as an additional variable. Off-shell effects in structure functions can be viewed as a way to describe in-medium modification of structure functions. This effect was discussed in terms of different approaches in the literature [13, 17, 14, 16, 19, 20]. Similar effects also hold for the structure functions xF_1 and xF_3.

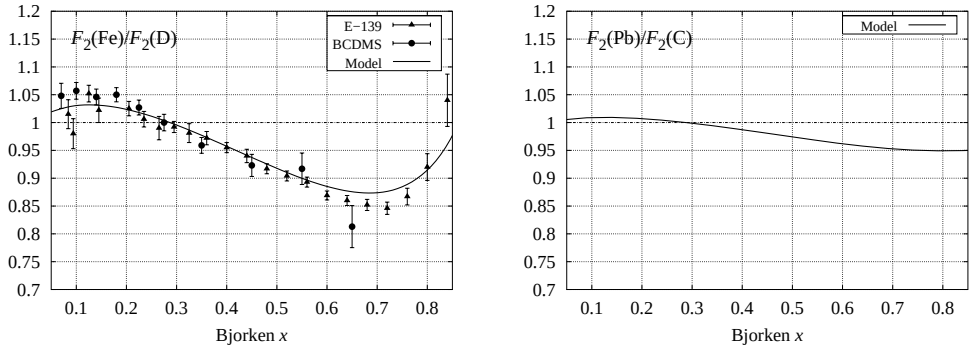

Figure 1: The ratio of iron to deuterium structure functions as measured by SLAC E-139 and CERN BCDMS collaborations in experiments with electron and muon beams (left panel). Also shown are the results of model calculation at fixed $Q^2 = 10\,\mathrm{GeV}^2$ which account for binding, Fermi-motion and off-shell effects in nuclear DIS [20]. The ratio of lead and carbon structure functions calculated at fixed $Q^2 = 10\,\mathrm{GeV}^2$ within the same approach is presented in the right panel.

Predictions of the convolution approach are compared to data on charged-lepton DIS in Fig. 1. Model calculations of nuclear structure functions use realistic nuclear spectral functions. Data seem to indicate that some off-shell modification of bound nucleon structure function is necessary [20]. The right panel of Fig. 1 displays the ratio of lead and carbon structure functions calculated within the same approach. One observes that nuclear effects at large x are practically saturated in

carbon. Similar nuclear effects are predicted for neutrino structure functions F_2 and xF_3. The MINERνA experiment will provide valuable information on nuclear effects in this region.

2.2 Nuclear effects at small x

Nuclear shadowing effects have been extensively discussed in the literature. A recent paper [7] provides a review of both experimental data and theoretical models of nuclear shadowing for charged-lepton scattering. This effect is interpreted as a result of the coherent interaction of the hadronic component of the virtual photons with a target nucleus. The structure functions at small x can be presented as a superposition of contributions from different hadronic states.

In fixed-target experiments the events with small Bjorken x are correlated with low invariant momentum transfer squared Q^2. At low Q^2 the vector meson dominance model (VMD) appears to be a good tool to study nuclear corrections in structure functions [7, 21]. In VMD the structure functions are saturated by contributions from a few low-mass vector meson states. For the interactions driven by the electromagnetic current usually only the isovector ρ and the isoscalar ω and ϕ mesons are important at low $Q^2 < 1\ \mathrm{GeV}^2$ [21]. The structure functions in this model have strong Q^2 dependence. In the generalized versions of VMD, the higher-mass states including continuum have also been considered that makes it possible to apply the model at higher Q^2 [7, 21].

The VMD approach has also been applied to weak interactions [22]. The vector current, in close analogy with the electromagnetic current, is assumed to be saturated by the ρ meson contribution at low Q^2. The axial-vector channel requires the consideration of contributions from the axial-vector meson a_1. However, there is a number of interesting physics questions related to the analysis of the axial-vector channel of neutrino interactions.

It should be emphasized that neutrino scattering at low Q^2 is dominated by contributions due to the axial current. Indeed, it is well known that contributions to the structure functions (cross sections) from the vector current vanish as $Q^2 \to 0$ because of vector current conservation. The axial current is not conserved and for this reason the longitudinal structure function F_L does not vanish at low Q^2. It was observed long ago by Adler that the neutrino cross sections at low Q^2 are dominated by the contribution from the divergence of the axial current [23]. The latter, because of PCAC, is saturated by the pion contribution. For this reason low Q^2 neutrino cross sections and structure functions are determined by pion cross sections. For the longitudinal structure function at low Q^2 the Adler relation is

$$2xF_L^{\mathrm{PCAC}} = \frac{f_\pi^2}{\pi}\sigma_\pi(s, Q^2), \tag{2}$$

where $f_\pi = 0.93 m_\pi$ is the pion decay constant (m_π is the pion mass) and $\sigma_\pi(s, Q^2)$ the total pion cross section at the center-of-mass energy $s = Q^2(1/x - 1) + M^2$ for

an off-shell pion with the mass squared Q^2. Equation (2) determines the dominant contribution to F_2 and neutrino production cross section at small Q^2 for nucleon and nuclear targets.

It is important to realize that Eq. (2) is not a consequence of the pion dominance of the axial current, i.e. fluctuation of the axial current to a pion which interacts with the target [26]. Indeed, the single-pion fluctuation of the axial current gives a vanishing contribution to the neutrino cross section. Instead, the axial current in neutrino interactions can produce heavy states such as the a_1 meson and $\rho\pi$ pair, which contribute to the interaction with the target. The overall contribution of all such states is described by the PCAC relation. The detailed mechanism of this phenomenon is not yet fully understood and the MINERνA experiment can provide new insights on physics driven by the axial current in neutrino interactions.

The strength of the nuclear shadowing effect is controlled by mesonic cross sections σ_v in the case of the vector current. In the axial-vector channel the relevant quantity is the pion cross section. In order to quantitatively understand nuclear effects, the multiple scattering effect on the cross section is calculated using Glauber–Gribov multiple scattering theory [24, 25, 21]. For a heavy nucleus the multiple scattering series can be written in a closed form (see, e.g. [21, 26])

$$\sigma_A = \sigma_N + \delta\sigma_A, \tag{3}$$

$$\delta\sigma_A = -\frac{\sigma_N^2}{2}\,\mathrm{Re}\int_{z_1<z_2} \mathrm{d}^2\boldsymbol{b}\mathrm{d}z_1\mathrm{d}z_2\,\rho(\boldsymbol{b},z_1)\rho(\boldsymbol{b},z_2)\exp\left[\int_{z_1}^{z_2}\mathrm{d}z'\left(\frac{i}{L_c}-\frac{\sigma_N}{2}\rho(\boldsymbol{b},z')\right)\right], \tag{4}$$

where σ_N and σ_A are the total cross sections of the hadronic state in question off the nucleon and the nucleus, respectively, and $\delta\sigma_A$ denotes the nuclear multiple scattering correction. In Eq. (4) ρ is the nucleon density distribution normalized to the number of nucleons and the integration is performed along the collision axis, which is chosen to be z-axis, and over the transverse positions of nucleons (impact parameter $\boldsymbol{b}$). L_c is the correlation length of the virtual hadronic state. The exponential factor in Eq. (4) accounts for multiple scattering effects. The rate of multiple scattering interactions is controlled by the mean free path of the hadronic fluctuation in a nucleus $l_f = (\rho\sigma)^{-1}$. If l_f is small enough compared with the nuclear radius, which is the case for heavy nuclei, then multiple scattering effects are important. It should be emphasized that the multiple scattering correction is negative because of the destructive interference of the forward scattering amplitudes on the upstream nucleons that causes *shadowing* of the virtual hadron interactions on the back-face nucleons.

If the correlation length is small compared to the average nuclear radius, $L_c \ll R$, then the oscillating factor in Eq. (4) suppresses multiple scattering corrections. The onset point of coherent nuclear effects can be estimated by comparing the coherence length of hadronic fluctuation L_c with the average distance between

bound nucleons in the nucleus d. For hadronic fluctuation of the vector current L_c is similar to the fluctuation time τ from Eq. (1), where m is the mass of hadronic state in question. The coherent nuclear effects take place if the fluctuation time is large enough $\tau > d$. This condition requires high energy transfer ν and, as is clear from Eq. (1), the coherent region comes earlier with energy for smaller masses m. However, it should be noted that, since for any mass of intermediate state $\tau < 2\nu/Q^2$, the region of coherent nuclear effects is limited to small x for any Q^2, $x < 1/Md$. Nuclear shadowing saturates if $L_c \gg R$, which happens at small x, and the condition $L_c \sim R$ defines the transition region with strong x dependence of the ratio $\delta\sigma_A/\sigma_N$.

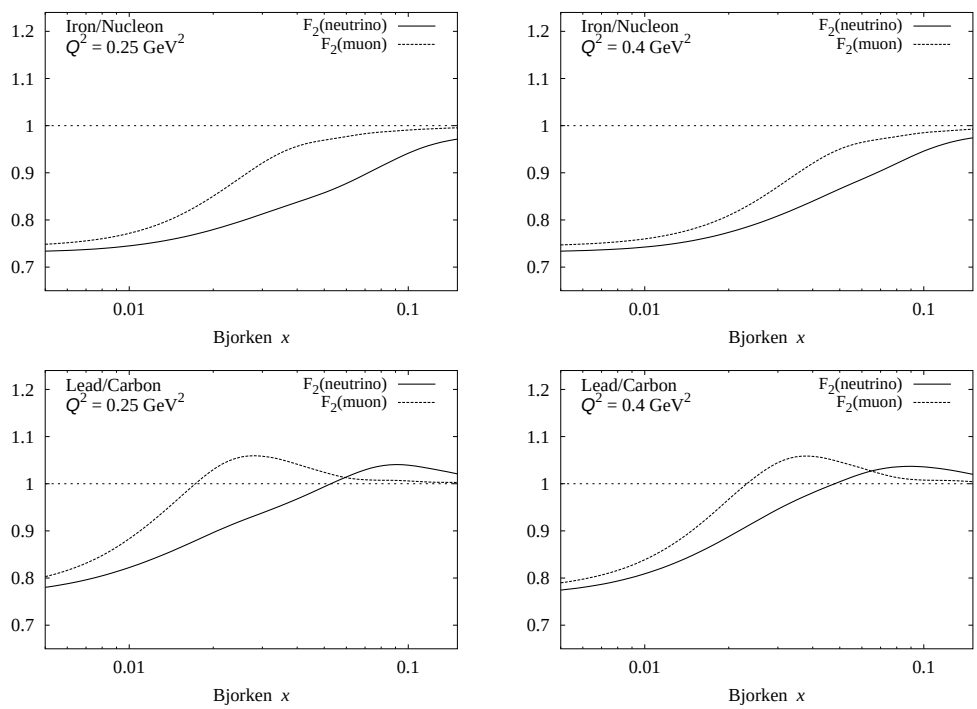

Figure 2: The ratio of iron to nucleon (upper row) and lead to carbon neutrino CC structure functions F_2^ν calculated at two different Q^2 within an approach based on PCAC and VMD (solid line). The dashed line shows similar ratios for the muon structure function F_2^μ.

For the axial-vector current neutrino interactions the fluctuation time τ is also given by Eq. (1). However, as was argued in [26], the fluctuation and coherence lengths are not the same in this case. In particular, the coherence length is determined by the pion mass m_π in Eq. (1) because of the dominance of off-diagonal transitions like $a_1 N \to \pi N$ in nuclear interactions. Since the pion mass is much smaller than typical masses of intermediate hadronic states for the vector current ($m_\rho,\ m_\omega$, etc.), the coherence length L_c of intermediate states of the axial current

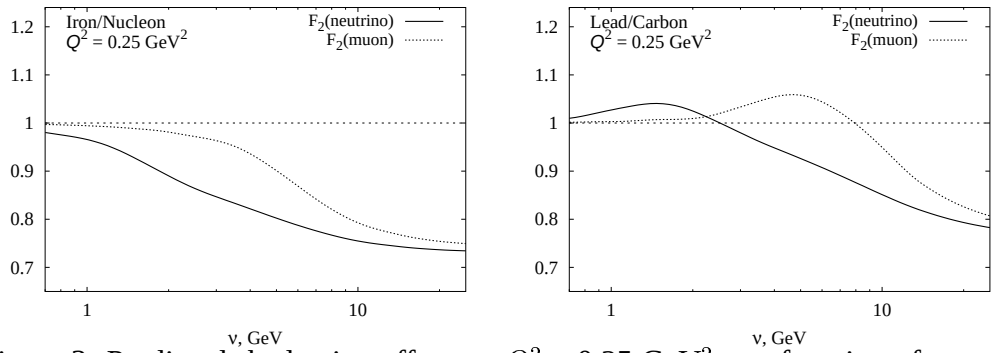

Figure 3: Predicted shadowing effects at Q^2 = 0.25 GeV^2 as a function of energy transfer (ν), for neutrinos (solid line) and muons (dotted line). The plot on the left is for iron compared to deuterium while the right plot is lead compared to carbon.

at low Q^2 will be much larger than L_c of the vector current. A direct consequence of this observation is early onset of nuclear shadowing effect in neutrino scattering at low energy and Q^2 compared with the shadowing in charged-lepton scattering.

Figure 2 shows the results of calculations of the ratios of iron to nucleon and lead to carbon structure functions calculated at two different Q^2 as a function of x. We also compare the nuclear shadowing effect for muon and neutrino scattering. The muon structure function was calculated using the VMD model of the electromagnetic current. Nuclear corrections to mesonic cross sections were calculated using Eq. (4) with the coherence length given by Eq. (1). The vector-current contribution to neutrino structure functions was also evaluated using the VMD model similar to the electromagnetic current case, while the axial-current contribution was treated using the PCAC relation (2). Nuclear corrections to the virtual pion cross section in (2) was evaluated by Eq. (4) assuming that the coherence length L_c is determined by the pion mass. One observes from these figures that the shadowing effect for neutrino interactions sets in earlier (at larger x) and its x-shape is different in the transition region of x between 0.1 and 0.01. The basic reason for the earlier onset of nuclear shadowing in neutrino scattering and different behavior in the transition region is the difference in the correlation lengths of hadronic fluctuations of the vector and axial-vector currents. This is also illustrated by observing that for a given Q^2 the cross-section suppression due to shadowing occurs for much lower energy transfer (ν) in neutrino interactions than for charged leptons. Figure 3 shows the predicted difference between neutrino and charged lepton shadowing as a function of the energy transfer (ν). On the left is the ratio of iron to deuterium while on the right is shown the ratio of lead to carbon.

The relative nuclear shadowing effect for the structure function F_3 is predicted to be substantially different from that for F_2 [27]. This is because the structure function F_3 describes the correlation between the vector and the axial-vector current in neutrino scattering. In terms of helicity cross sections, the structure function F_3 is given by the cross section asymmetry between the left- and right-polarized states of the virtual W boson. It is known that such a difference of cross

sections is strongly affected by Glauber multiple scattering corrections in nuclei. This causes an enhanced nuclear shadowing effect for the structure function F_3.

The results for the ratio of lead and carbon structure functions are shown in Fig. 4. Unlike nuclear effects at large Bjorken x, which are shown in Fig. 1, one observes substantial, structure function dependent, nuclear effects at small x. The MINERνA experiment can provide a unique tool to study these effects.

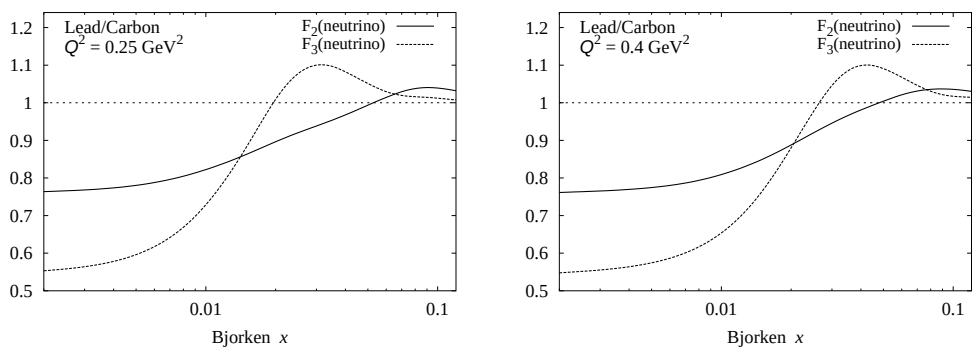

Figure 4: The ratio of lead and carbon neutrino CC structure functions F_2 calculated in an approach based on PCAC and VMD at two different Q^2 (solid line). Similar ratio for the structure function xF_3 is shown by the dashed curve.

2.3 Nuclear effects and determination of $\sin^2\theta_W$

The rate of neutral-current (anti)neutrino scattering is directly determined by the value of $\sin^2\theta_W$. Therefore the measurement of NC/CC ratios of neutrino cross sections provides a valuable tool for the determination of $\sin^2\theta_W$. For an isoscalar target (e.g. the isoscalar combination of proton and neutron, or for deuterium) a relation between neutrino–antineutrino asymmetries in the NC and CC DIS cross sections was derived by Paschos and Wolfenstein [28]

$$R^- = \frac{\sigma^\nu_{\rm NC} - \sigma^{\bar\nu}_{\rm NC}}{\sigma^\nu_{\rm CC} - \sigma^{\bar\nu}_{\rm CC}} = \frac{1}{2} - \sin^2\theta_W, \tag{5}$$

where θ_W is the Weinberg mixing angle. A similar relation also holds for the NC/CC ratio of the structure functions

$$F_3^{\rm NC}(x,Q^2)/F_3^{\rm CC}(x,Q^2) = 1 - 2\sin^2\theta_W, \tag{6}$$

where $F_3^{\rm CC}$ is the neutrino and antineutrino averaged structure function, $F_3^{\rm CC} = (F_3^\nu + F_3^{\bar\nu})$.

It should be stressed that if only the contributions due to light quarks are taken into account, then the PW relationship is a direct result of isospin symmetry. This

ensures that various strong interaction effects, including nuclear effects, cancel out in R^- for an isoscalar target thus making Eq. (5) a good tool for the measurement of the mixing angle in neutrino scattering.

The targets used in neutrino experiments are usually heavy nuclei, such as iron in the NuTeV experiment [29]. Heavy nuclei typically have an excess of neutrons over protons and, therefore, are not isoscalar targets. For a non-isoscalar target the relations (5) and (6) are violated by contributions due to isovector components of nuclear parton distribution functions. Nuclear corrections to relations (5) and (6) were recently studied in [30, 31, 32]. It was shown that nuclear effects enter through non-isoscalar effects in the target. These studies suggests that nuclear corrections can be greatly reduced when using isoscalar targets such as carbon. MINERνA, with its lead, iron, and carbon targets, will be able to directly measure the ratio NC/CC for various nuclear targets to explore these nuclear effects experimentally.

3 Final-State Interactions (FSI) in Neutrino Interactions

Interactions of few GeV neutrinos in nuclei easily produce resonances which decay to pions. Any attempt to reconstruct the incident neutrino energy based on the total observed energy must take into account the interactions of the pions within the interaction nucleus. Current neutrino interaction Monte Carlos (such as INTRANUKE [33]) handle intra-nuclear pion interactions crudely and have generally not yet incorporated the latest knowledge of pion interactions.

The concern is mainly with pions in the energy range of 100 to 500 MeV, where the interaction cross sections are the highest. In this range the pion-nucleon cross section is dominated by the very strong $\Delta(1232)$ resonance. The Δ is a fairly broad (about 100 MeV) resonance, and the pion-nucleon cross section reflects this, with a peak near 200 MeV pion energy which drops quickly above and below this. The pion nucleus cross section exhibits a similar behavior, with a less pronounced drop-off at higher energy. The charged pion nucleus cross section has four important components in the intermediate energy range: elastic scattering (nucleus left in the ground state), inelastic scattering (nucleus left in an excited state or nucleon knocked out), true absorption (no pion in the final state), and single charge exchange (neutral pion in the final state).

Neutrino detectors are mainly iron (absorber), oxygen (water) and carbon (scintillator). The total pion-carbon cross section is 600 mb, with elastic and inelastic cross sections about 200 mb each, and absorption about 160 mb. The total pion-iron cross section is about 1700 mb, with elastic and absorption about 600 mb each, and inelastic about 400 mb. Cross sections for positive and negative pions are nearly the same because nuclei contain about the same number of

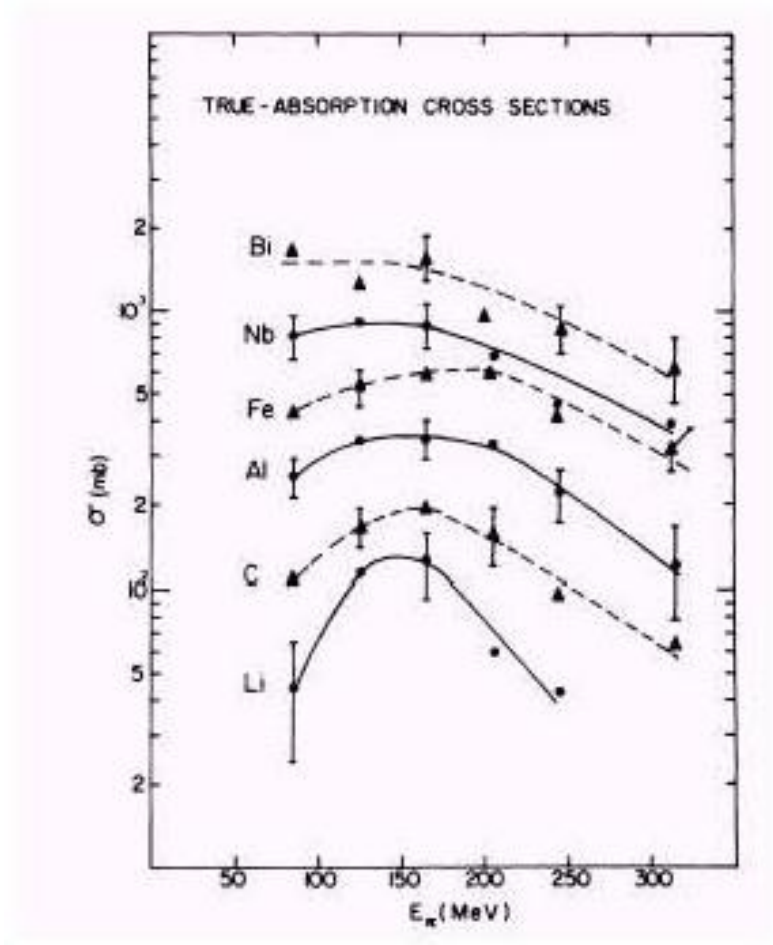

Figure 5: The absorption cross-sections for various nuclei as a function of pion energy.

protons and neutrons. These very large cross sections mean that essentially many pions will undergo some nuclear reaction within the interaction nucleus. In elastic and most inelastic reactions the scattered pion will not, because of its light mass, lose much energy. However, absorbed pions will lose all of their kinetic and mass energy. Of the four components of this intra-nuclear cross-section, the absorption probability within the interaction nucleus is order 30%. Figure 5 [34] shows absorption cross sections for various nuclei as a function of pion energy.

Pion absorption cannot occur on a single nucleon due to energy and momentum conservation. The simplest absorption mechanism is on two nucleons. Because absorption appears to proceed mainly through the $N-\Delta$ intermediate states, an isospin zero (np) pair is the primary candidate. Such an absorption for a positive pion would give two energetic protons whose kinetic energy nearly equaled the total pion energy. However, early studies of pion absorption found that was

not the most probable mechanism.

In the 1990's two large solid angle detectors, the LAMPF BGO Ball and the PSI LADS detector, were built to study pion absorption. Both detectors had large solid angles (both more than 90% of the full solid angle) and low proton thresholds (about 20 MeV for each). The LADS detector also had reasonable neutron detection efficiency and energy measurement. The somewhat surprising result from both detectors was that pion absorption was dominated by three body absorption [35]. For positive pions, the absorption on a pnn triplet (leading to a ppn final state) was the most common. This was observed even in ^{4}He. The absorption in heavier nuclei also appears to proceed mainly through a three-body mechanism, although increased initial state interactions (pion re-scattering) and final state interactions (nucleon re-scattering) result in four to five nucleons being emitted. Typically the final state contains more neutrons than protons. The absorption process, which is still not well understood theoretically, largely fills the available phase space thus giving a wide range of nucleon energies with little angular dependence.

Because much of the energy is in neutrons, the observed energy is well below the total pion energy. Figure 6 and Figure 7 [36] show missing energy (total pion energy minus the total proton kinetic energy) for absorption of 250-500 MeV positive pions on ^{12}C and ^{58}Ni. As can be seen, even in carbon more than half the energy is lost to unobserved particles, a fraction which increases with pion energy and with A.

The situation is of course worse for negative pions. Charge symmetry would indicate that the primary absorption should be on a ppn triplet leading to a pnn final state. In this case, most of the pion energy would be in neutrons, and hence not directly observed. However, if the interaction vertex and one proton energy is known, and the angles of the outgoing neutrons are known, the total energy of the three nucleons can be estimated. Monte Carlo studies with realistic absorption models will be needed to determine the accuracies of such estimates.

Although neutral pions escaping the nucleus will decay, usually to two photons, the mean distance traveled before decay is a few nanometers, much greater than the size of the nucleus. Thus the absorption of neutral pions in the interaction nucleus must also be taken into account in any study of resonance production.

For MINERνA, studies with INTRANUKE have begun to determine the sensitivity to the probability of pion absorption in the interaction nucleus. Monte Carlo routines are being modified to treat pion absorption more realistically. Note also that there are essentially no measurements of pion absorption above 500 MeV. The fine spatial resolution and full solid angle detection capability of MINERνA will allow a study of these interactions, especially in carbon.

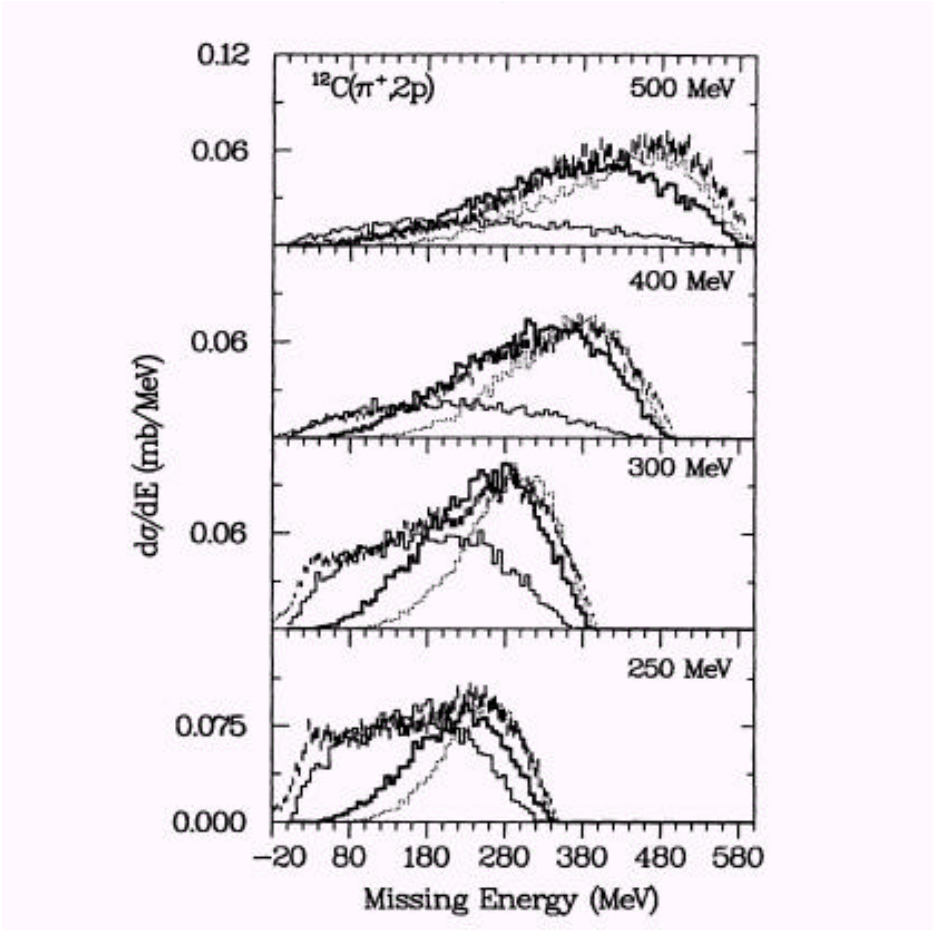

Figure 6: The missing energy (total pion energy minus the total proton kinetic energy) for the absorption of 250-500 MeV pions on carbon.

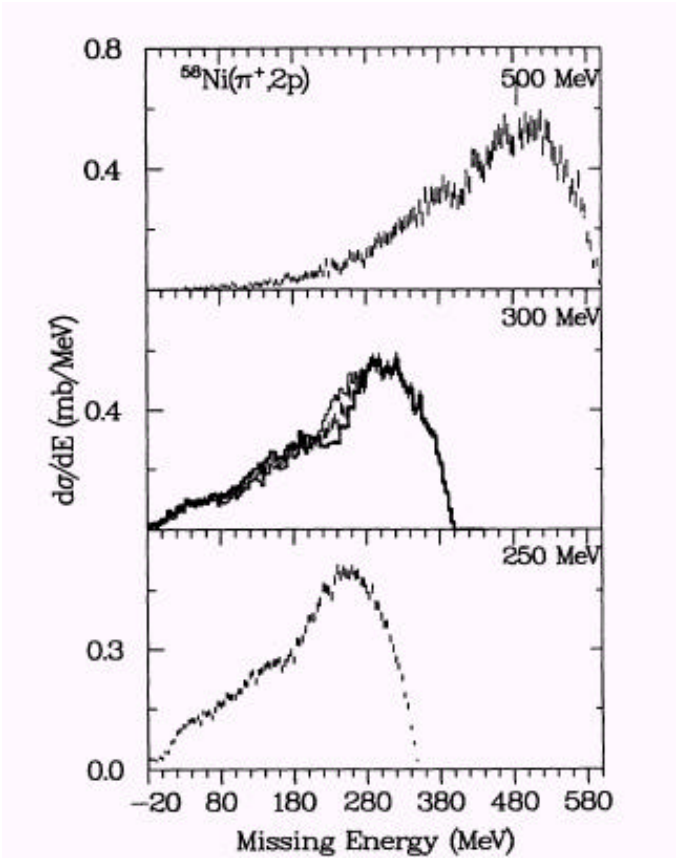

Figure 7: The missing energy (total pion energy minus the total proton kinetic energy) for the absorption of 250-500 MeV pions on nickel.

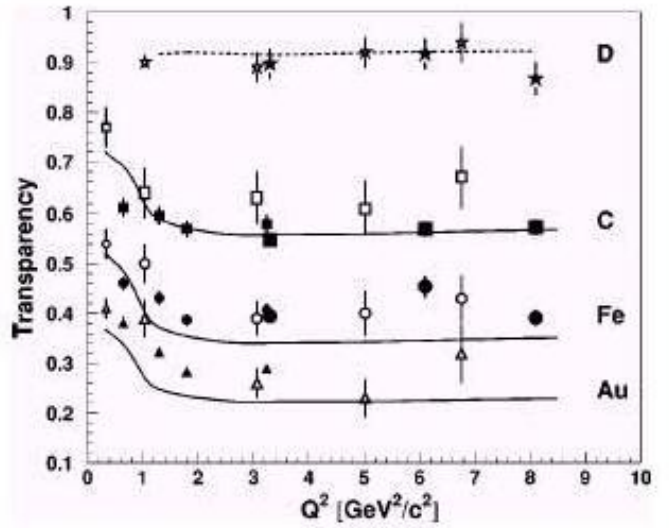

Figure 8: Probability for the outgoing proton to escape the nucleus as a function of Q^2.

3.1 Nuclear Transparency in Neutrino Interactions

A second nuclear interaction process which affects the observed final state energy is the final state interaction of a nucleon in the struck nucleus. An outgoing nucleon has a substantial probability of interacting in the nucleus. These probabilities have been measured, most recently at JLab, with some precision. The experiments used $(e, e'p)$ coincidence reactions. The cross section for finding the scattered electron in the quasi-elastic peak was compared to the cross section for finding the coincident proton. A summary of the results are shown in Fig. 8.

In contrast to pion absorption, there is little available information on what happens to the scattered nucleon. Of course, most either scatter from a single nucleon quasi-elastically or produce a pion (for protons above 600 MeV). Improving Monte Carlo routines to model this interaction should allow us to better estimate the total final state energy. As with pion absorption, the good resolution, neutron detection capability, and full solid angle coverage of MINERνA should allow experimental determination of the actual final states and help constrain the Monte Carlo routines.

4 Measuring Nuclear Effects with the MINERνA Detector

To study nuclear effects in MINERνA, carbon, iron and lead targets will be installed upstream of the pure scintillator active detector. The currently preferred

configuration involves a total of 9 planes, with each plane divided transversely into C, Fe and Pb wedges. As one proceeds from upstream to downstream, the C, Fe and Pb targets exchange (rotate) positions. A scintillator module of four views (x,u,x,v) separates each of the planes. The total mass is over 1 ton of Fe and Pb and somewhat over 0.5 ton of C. Since the pure scintillator active detector essentially acts as an additional 3-5 ton carbon target (CH), the pure graphite (C) target is mainly to check for consistency. For the standard four-year run described in the proposal, MINERνA would collect over 740 K events on Fe and Pb, 430 K events on C as well as 2.3 M events on the scintillator within the fiducial volume.

MINERνA's goals in measuring nuclear effects can be summarized as follows:

- measure final-state multiplicities, and hence absorption probabilities, as a function of A with initial ν;
- measure the visible hadron energy distribution as a function of target nucleus to determine the relative energy loss;
- investigate if the correction factors for observed multiplicity and hadron energy are a function of the muon kinematics for a more directed application of nuclear effect corrections;
- measure $\sigma(x,\ Q^2)$ for each nuclear target to compare x-dependent nuclear effects measured with both ν and charged lepton beams;
- measure the nuclear effects on $F_2(x,\mathrm{Q}^2)$ and $xF_3(x,Q^2)$ to determine whether sea and valence quarks are affected differently by the nuclear environment.

4.1 Proposed Experimental Analysis - modified interaction probabilities

To measure this nuclear effect, the cross-section and resulting structure functions $F_2(x,Q^2)$ and $xF_3(x,Q^2)$ will be measured for the three target nuclei of C, Fe and Pb. For the standard 4-year run we expect around 740 K events per target distributed in x depending on the W-region in question. For an A-dependent comparison in the DIS region (W $\geq$ 2 GeV and $Q^2 \geq$ 1 GeV^2) we would have 330 K events per target with 66 K events per target in the shadowing region ($x \leq 0.1$) and 20 K events per target in the high x region $(x \geq 0.5)$.

To study the axial-vector nuclear shadowing effects expected at low Q^2 (non-DIS events) and low ν we will have 133 K events per target with $Q^2 \leq$ 1.0 GeV^2 and $x \leq 0.1$. For example, the expected distribution of events with $Q^2 \leq 0.4$ GeV^2 and $\nu \geq$ 6 GeV (the region of maximal predicted difference with respect to charged lepton shadowing) is shown in Fig. 9. With these expected statistics, MINERνA should be able to measure the expected difference in lead to carbon shadowing for charged leptons compared to ν's to just under 3 standard deviations statistically.

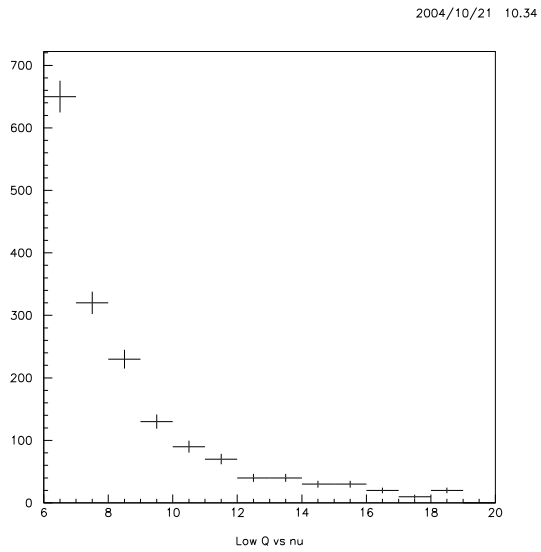

Figure 9: The expected event sample per target with $Q^2 \leq 0.4\text{GeV}^2$ and $\nu \geq 6$ GeV.

4.2 Proposed Experimental Analysis - final state interactions in neutrino production

The NEUGEN Monte Carlo has been used to study the sensitivity of the MINERνA experiment to nuclear effects. The nuclear effects in the NEUGEN Monte Carlo are controlled by the INTRANUKE processor. This processor incorporates a probability for pion absorption based on earlier electroproduction absorption studies and lower-statistics Ne/H_2 neutrino bubble chamber data. The observed phenomena of hadron formation length, which increases the transparency and reduces final state interactions, is incorporated as well. The particular model used for pion absorption, which is currently being improved and updated, assumes that the absorption process eliminates a pion and the resulting nucleons are themselves either absorbed in the nucleus or are too low in energy to be observed in the detector.

To determine the sensitivity of MINERνA measurements to the predictions of this model, the assumed probability for pion absorption in INTRANUKE has been increased by three standard deviations and then decreased by the same amount that, essentially, turns off pion absorption. The multiplicity and a simple, crude estimate of the visible hadron energy have been examined under these extreme conditions. Note that other nuclear effects such as intra-nuclear scattering and hadron formation length have not been changed from their nominal values. Figure 10 shows both the truth and reconstructed multiplicity distributions for carbon. As can be seen, the available crude tracker fails to reconstruct many of the tracks. We expect this problem to be significantly resolved when full pattern recognition and a more sophisticated tracker become available. For the current study, we will use the truth value of multiplicity.

In the next series of figures the predicted asymmetry in the true multiplicity

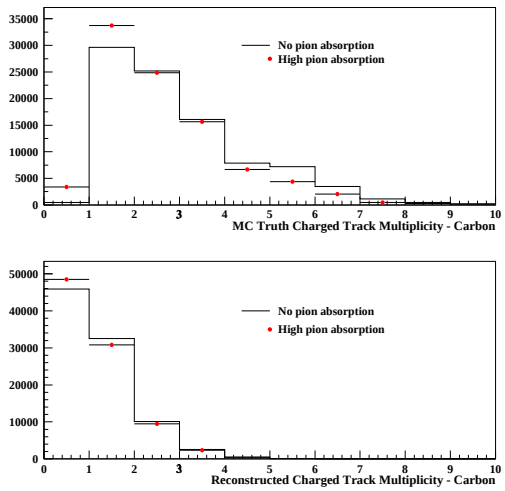

Figure 10: The shift in the truth and reconstructed multiplicity distributions between the two values assumed for pion absorption on carbon described in the text.

and visible hadron energy are shown. The asymmetry is defined as the percentage change under these extreme assumptions. That is, the bin contents at plus three standard deviations minus the bin contents at minus three standard divided by bin contents at minus three standard deviations. Figure 11 shows the asymmetry in the true multiplicity for carbon, while Fig. 12 and Fig. 13 shows the same distribution for iron and lead respectively. One sees a rather dramatic effect for carbon as the high absorption value has increased the number of 0-track events by over a factor of 6 compared to the no-absorption case. This is due to the fact that the other nuclear effects, not being changed, are minimal for carbon. Since intranuclear rescattering increases as $A^{1/3}$ and the reduction of nuclear effects due to hadron formation length decreases as $A^{1/3}$, the non-absorption nuclear effects are minimal for carbon and already sizable for iron and lead If this model is realistic, the carbon multiplicity distribution should be quite sensitive to the probability of absorption.

The final determination of the visible hadron energy will be an involved process for this experiment. For now, we are using the most primitive estimate of this quantity, namely an uncorrected version derived from the total light output of the hadron shower. In the data analysis this will be refined for example, through measurements of stopping/decaying particles. With this crude estimate, the change in hadron energy for iron is shown in Fig. 14 and for lead in Fig. 15. There is a significant increase in the number of events with E_H less than 3 GeV and a corresponding decrease in the number of events with higher E_H as one would expect. MINERνA will collect several times these statistics and should be capable of measuring this effect at even higher hadron energy.

Since the incoming neutrino energy is not *a priori* known, the measured **muon**

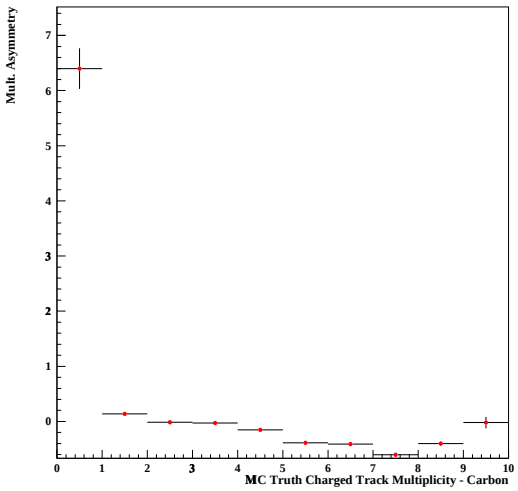

Figure 11: The fractional change in true multiplicity distributions between the two values assumed for pion absorption on carbon described in the text.

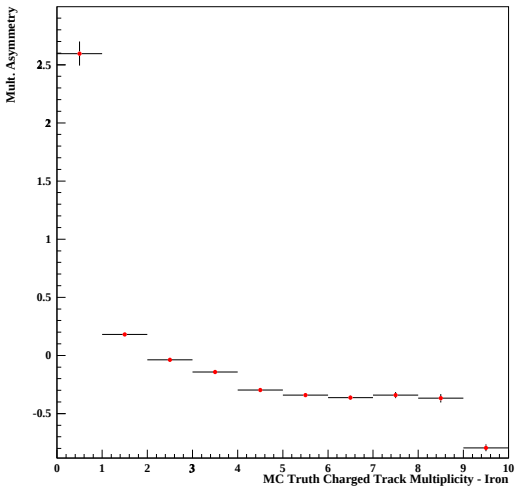

Figure 12: The fractional change in true multiplicity distributions between the two values assumed for pion absorption on iron discussed in the text.

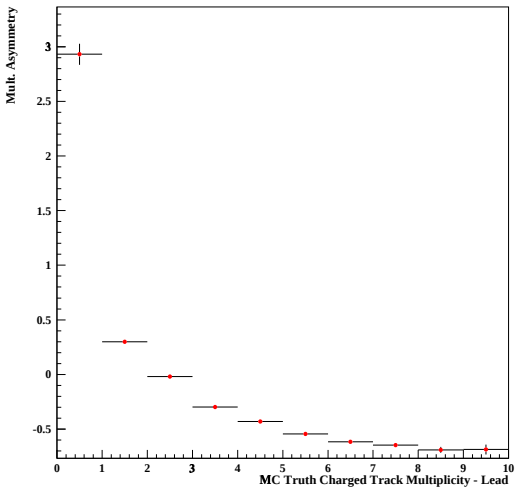

Figure 13: The fractional change in true multiplicity distributions between the two values assumed for pion absorption on lead discussed in the text.

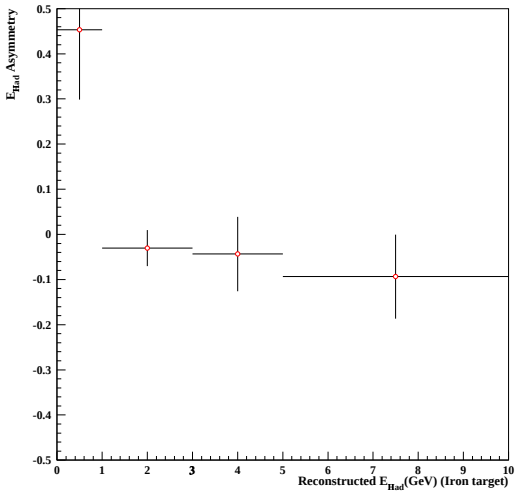

Figure 14: The fractional change in the visible hadron energy distributions between the two values of pion absorption on iron discussed in the text.

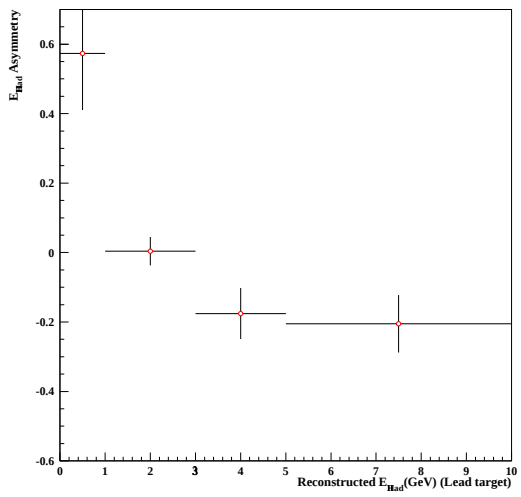

Figure 15: The fractional change in the visible hadron energy distributions between the two extremes in pion absorption on lead discussed in the text.

kinematics will be tested as a basis to compare characteristics of the visible hadron shower across nuclear targets and to determine whether a nuclear-effects correction-factor as a function of the observed muon kinematics cam bee determined. The muon is relatively free from nuclear dependent effects and serves well as an A-independent normalization. For example, the quantity:

$$Q' = E_\mu \sin^2(\theta/2) \tag{7}$$

is representative of the 4-momentum transfer to the nucleon or quark (divided by E_ν) and reflects the energy-momentum transferred to the hadronic vertex. The distribution of events in this quantity is peaked toward low Q'. with half the events below Q' = 1.0 GeV.

References

[1] D. Drakoulakos *et al.* [Minerva Collaboration], arXiv:hep-ex/0405002. Pgs. 99 - 108, 192 - 200.

[2] B.Z. Kopeliovich, hep-ph/0409079.

[3] M.K. Jones *et al.*, Phys. Rev. **C48**, 2800 (1993); R.D. Ransome *et al.*, Phys. Rev. **C46**, 273 (1992); R.D. Ransome *et al.*, Phys. Rev. **C45**, R509 (1992).

[4] D. Rowntree *et al.*, Phys. Rev. **C60**, 054610 (1999); B. Kotlinksi *et al.*, Eur. Phys. J. **A9**, 537 (2000).

[5] E. A. Paschos, M. Sakuda, I. Schienbein and J. Y. Yu, arXiv:hep-ph/0408185.

[6] M. Arneodo, Phys. Rept. **240**, 301 (1994).

[7] G. Piller and W. Weise, Phys. Rept. **330**, 1 (2000).

[8] B. L. Ioffe, V. A. Khoze, and L. N. Lipatov, *Hard processes: Phenomenology, Quark-Parton Model* (Elsevier Science Publishers, North Holland, 1984).

[9] G.B. West, Ann. Phys. **74** (1972) 464.

[10] S. V. Akulinichev, S. A. Kulagin, and G. M. Vagradov, Phys. Lett. B **158**, 485 (1985); S. V. Akulinichev, S. Shlomo, S. A. Kulagin, and G. M. Vagradov, Phys. Rev. Lett. **55**, 2239 (1985).

[11] S. A. Kulagin, Nucl. Phys. A **500**, 653 (1989).

[12] C. Ciofi degli Atti and S. Liuti, Phys. Rev. C **41**, 1100 (1990).

[13] F. Gross and S. Liuti, Phys. Rev. C **45**, 1374 (1992).

[14] S. A. Kulagin, G. Piller and W. Weise, Phys. Rev. C **50**, 1154 (1994).

[15] S. A. Kulagin, W. Melnitchouk, G. Piller, and W. Weise, Phys. Rev. C **52**, 932 (1995).

[16] S. A. Kulagin, Nucl. Phys. A **A 640**, 435 (1998).

[17] W. Melnitchouk, A. W. Schreiber and A. W. Thomas, Phys. Rev. D **49**, 1183 (1994).

[18] J. Gomez, *et al.*, Phys. Rev. D **49**, 4348 (1994).

[19] S. I. Alekhin, S. A. Kulagin and S. Liuti, Phys Rev. D **69**, 114009 (2004).

[20] S. A. Kulagin and R. Petti, paper in preparation.

[21] T. H. Bauer, R. D. Spital, D. R. Yennie and F. M. Pipkin, Rev. Mod. Phys. **50**, 261 (1978) [Erratum-ibid. **51**, 407 (1979)].

[22] C. A. Pickety, and L. Stodolsky, Nucl. Phys. B **15**, 571 (1970).

[23] S. L. Adler, Phys. Rev. **135**, B963 (1964).

[24] R. J. Glauber, Phys. Rev. **100**, 242 (1955).

[25] V. N. Gribov, Sov. Phys. JETP **29**, 483 (1970) [Zh. Eksp. Teor. Fiz. **56**, 892 (1969)]; Sov. Phys. JETP **30**, 709 (1970) [Zh. Eksp. Teor. Fiz. **57**, 1306 (1969)].

[26] B. Z. Kopeliovich, and P. Marage, Int. J. Mod. Phys. A **8**, 1513 (1993).

[27] S. A. Kulagin, arXiv:hep-ph/9812532.

[28] E. A. Paschos and L. Wolfenstein, Phys. Rev. D **7**, 91 (1973).

[29] G. P. Zeller *et al.* [NuTeV Collaboration], Phys. Rev. Lett. **88**, 091802 (2002) [Erratum-ibid. **90**, 239902 (2003)] [arXiv:hep-ex/0110059].

[30] S. A. Kulagin, Phys. Rev. D **67**, 091301 (2003) [arXiv:hep-ph/0301045].

[31] S. A. Kulagin, arXiv:hep-ph/0406220.

[32] S. A. Kulagin, arXiv:hep-ph/0409057.

[33] R. Merenyi *et al.*, Phys. Rev. D **45**, 743 (1992), W. A. Mann *et al.*, unpublished.

[34] D. Ashery *et al.*, Phys. Rev. C **23**, 2173 (1981).

[35] C.H.Q. Ingram, Nucl. Phys. A **684**, 122 (2001).

[36] M. K. Jones *et al.*, Phys. Rev. C **48**, 2800 (1993).